

Article

Predicting Unconfined Compressive Strength Decrease of Carbonate Building Materials against Frost Attack Using Nondestructive Physical Tests

Marzouk Mohamed Aly Abdelhamid ^{1,2}, Dong Li ¹ and Gaofeng Ren ^{1,3,*}

¹ School of Resources and Environmental Engineering, Wuhan University of Technology, Luoshi Road 122, Wuhan 430070, China; eng.mohamedali@whut.edu.cn (M.M.A.A.); lidong_whut@163.com (D.L.)

² Faculty of Engineering, Mining and Petroleum Engineering Department, Al-Azhar University, Cairo 11884, Egypt

³ Key Laboratory of Mineral Resources Processing and Environment of Hubei Province, Luoshi Road 122, Wuhan 430070, China

* Correspondence: rengf110@whut.edu.cn; Tel.: +86-18986194926

Received: 23 January 2020; Accepted: 9 February 2020; Published: 13 February 2020



Abstract: Carbonate building materials and engineering constructions are exposed to severe seasonal environmental fluctuations and result in a full or partial disintegration, especially in cold regions, and employment of nondestructive methods for evaluating the durability of building materials subject to frost weathering is gaining great significance. This research aims to obtain reliable relationships between unconfined compressive strength decrease and nondestructive parameters variations of limestone types under frost conditions and provide useful information regarding their durability in order to ensure the long-term viability or sustainability of these materials used for constructions against frost conditions. In this study, five important types of Chinese limestone used as construction materials were subjected to 50 frost cycles. Unconfined compressive strength, compressional wave velocity and spatial attenuation, and porosity were obtained at the end of every 10 cycles. As a result of progression in frost cycles, the increase and decrease rates were determined at the end of every 10 cycles, and the relationships between them were obtained to predict the loss ratios of unconfined compressive strength ($RD\sigma_c$). Results indicated that at the end of 40th cycles, there was a high correlation between $RD\sigma_c$ and spatial attenuation loss with an R^2 of 0.8584. Furthermore, there was also a strong relationship between $RD\sigma_c$ and compressional wave velocity decrease after the end of 20th and 50th cycles with an R^2 of 0.9089 and 0.9025, respectively. Therefore, these relations are reliable to provide useful information for durability and viability of studied samples under frost conditions and support the use of the ultrasonic measurements. It can also be successfully used for pre-estimation of unconfined compressive strength loss of studied limestone types against frost weathering without any tests.

Keywords: frost weathering; unconfined compressive strength; compressional wave velocity; spatial attenuation; durability; sustainable building materials; Limestone

1. Introduction

Degradation of stones used as building and construction materials under severe environmental conditions is very important for many applications such as railroads, roads, and rock slopes, especially in cold areas [1–7]. Natural rocks are subject to at least one freezing–thawing cycle annually. These repeated cycles lead to rapid changes in engineering characteristics and hence limit rock durability in the course of time [8]. Rock damage in cold regions is influenced by a number of frost weathering cycles, rock types, temperatures, applied pressures, and rock parameters including mineral content,

porosity, and pore size distribution [9,10]. When water turns into ice, it expands in volume by up to 9%, thus giving rise to an increase in the stress inside the pores. When the stress reaches the tensile strength of the rock, new micro-cracks are formed, and the present ones are deepened and widened; therefore, these changes can influence the rock mechanical properties and its durability [11,12]. The physical, mechanical, and petrographical properties of rocks are very important in the selection of natural stones used as construction and building materials subject to freezing–thawing weathering [13]. Characterizations of petrographical properties are significant tools to evaluate the durability of rock materials against accelerated weathering agents and provide information about the mineralogical composition and textural properties and provenance of the rock materials' origins [6].

Fort et al. [14] used Schmidt hardness and ultrasound velocity for in situ testing of rock characteristics of stone monuments and their quarries. They concluded that the results of these two nondestructive tests are reliable indicators of the degree of rock deterioration. Takarli et al. [10] studied the influence of freezing–thawing cycles on microstructure in saturated granitic rocks by testing compression wave velocity and permeability. They founded that a decrease in compressional wave velocity and permeability measurements for these rocks. However, Martínez-Martínez et al. [15,16] and Hashemi et al. [17] reported that the spatial attenuation is more sensitive ultrasonic property for detecting damage processes in carbonate building stones. Yavuz et al. [18] established a model to evaluate the index parameters (compressional wave velocity, Schmidt rebound and mechanical unconfined compressive strength) of deteriorated carbonate rocks from the initial index properties after 20 freezing–thawing cycles. Saad et al. [19] studied the effect of water flows into porous network on freezing–thawing cycles of rocks. Karaca et al. [20] experimentally studied the Böhme abrasion and wide-wheel abrasion parameters before and after frost weathering tests. They proposed the statistical models for abrasion values before and after frost cycles. Tan et al. [21] investigated the deterioration in the mechanical characteristics of granite as a function of freezing–thawing processes by uniaxial and triaxial compression tests. Mutluturk et al. [22] postulated a mathematical model to predict the decrease of integrity process of rocks due to freezing–thawing processes and provided different meaningful properties for rock decay or rock durability. Sousa et al. [23] derived an empirical formula between the rock strength and porosity for a sample of granitic rocks. Bayram [24] developed a statistical model to predict the rate of decrease values in uniaxial compressive strength. In this model, impact strength, elastic modulus, and absorption of water were used as independent variables. Baud et al. [24] proposed an analytical model in which unconfined compressive strength, initial porosity, and crack density in a rock were related. Many studies investigated the decay of physico-mechanical properties of rocks due to freezing–thawing action [10,16,18,21,25–31].

In the previous works, estimation of damaged stones used as building and construction material due to freezing–thawing conditions were classified into two groups—physical and mechanical. The physical parameters mainly include compressional wave velocity, porosity, and mass, which can be noninvasively measured. The destructive mechanical parameters include compressive strength, modulus of elasticity, tensile strength, and impact strength. The destructive mechanical test of rock materials due to freezing–thawing action is the most direct and plain method for estimating the uniaxial compressive strength decrease for stones used for building and constructions. Unconfined compressive strength is the most important mechanical method to determine the strength of materials. However, it is time-consuming, expensive, and sample preparation is difficult. The strength loss of rock materials against frost conditions is an important indicator to select stones for building and construction purposes and assess the stability of rock engineering in cold regions. Therefore, predicting the strength parameters by the other physical and mechanical nondestructive test methods is popular and preferable. However, most of the previous studies are focused on destructive mechanical tests and some different numerical methods. Therefore, these tests are insufficient to predict the unconfined compressive strength of carbonate building materials due to frost weathering process. Moreover, this test is generally applied with natural environmental conditions.

Our current research aims to predict the unconfined compressive strength loss from nondestructive physical tests of some carbonate building materials such as limestone against frost weathering. Specifically, it aims to obtain significant or reliable relationships between unconfined compressive strength decrease and nondestructive parameters variations including compressional wave velocity, spatial attenuation, and porosity of studied materials. It also, aims to provide useful information regarding their durability in order to ensure the long-term viability or sustainability of these materials used for constructions against frost weathering conditions.

The remainder of this paper is organized as follows. In Section 2, materials description, and laboratory experiments setup details such as petrographic analysis, frost attack process, unconfined compression test, porosity, water absorption, and ultrasonic detection system are presented. Section 3 presents the results and discussions in addition to evaluation of the relationships between $RD\sigma_c$ and some nondestructive properties of studied limestone samples. Finally, conclusions are drawn in Section 4.

2. Materials and Methods

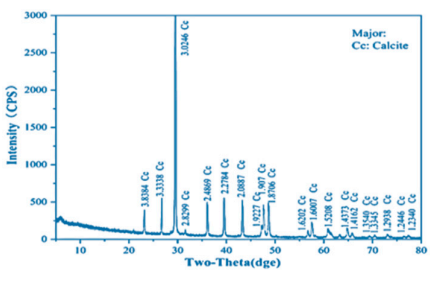
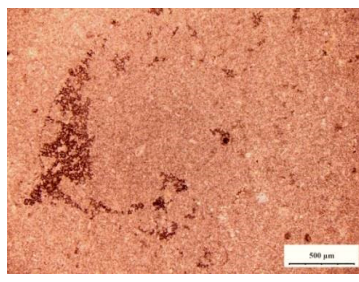
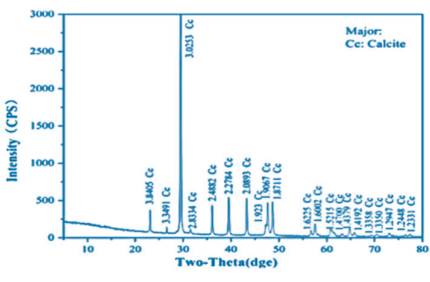
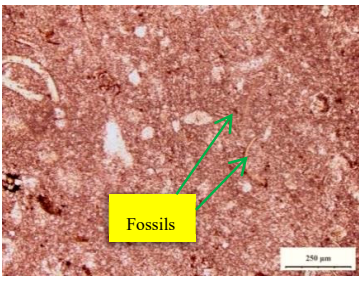
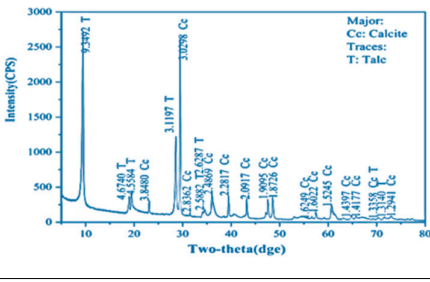
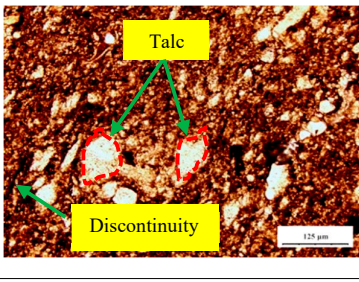
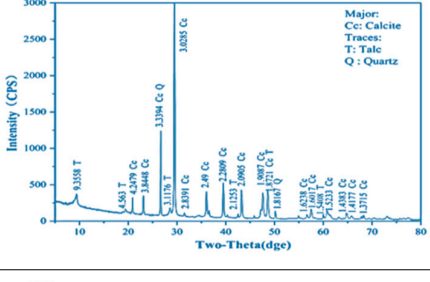
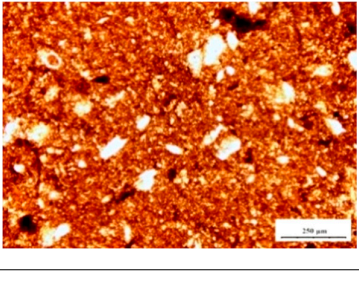
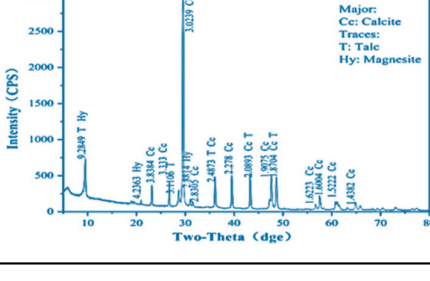
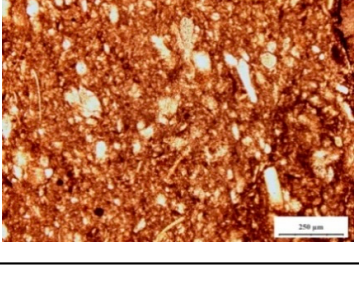
2.1. Raw Materials

Five different types of limestone used as building and constructions materials in Hubei Province, China, were used in this study. Limestone samples were prepared in a cylindrical shape with a diameter of 50 mm and tested before and after frost attack processes. The studied limestone samples were free from any defects, including bedding planes, fractures, and weathering, in order to eliminate the effect of anisotropy on the measurement. The number of samples used for tests was 180 samples. Two series of specimens were prepared in this study; one set of these specimens was used to determine the initial physical and mechanical characteristics before frost weathering cycles, and the second set of specimens was subjected to frost cycles to determine some nondestructive engineering characteristics including ultrasonic measurements (compressional wave velocity and spatial attenuation), porosity, and unconfined compressive strength.

2.2. Petrographic Properties

The X-ray diffraction (XRD) and polarized optical microscope (POM) analysis were used to identify the mineralogical composition and the microstructure characteristics of the different limestone samples. Thin section studies indicated that the studied rocks consist mainly of calcite as major mineral component and represent more than 90%, while some of them have accessory minerals such as talc, magnesite, and quartz in their mineralogical composition. The major petrographic analysis of studied specimens is given in Table 1. As shown in this table, CK-H1 limestone samples consist mainly of calcite as main mineral constituent associated with some rare amounts of opaque minerals. Calcite mineral appears as a fine-grained texture. ZK01-H1 samples have a fine-grained texture and are composed of calcite, an essential component that represents the cement of the rock materials associated with low amounts of opaque minerals. Very fine fossils were presented in this rock. ZK01-H2 samples were coarse grained in texture and were composed mainly of calcite as their major mineral constituent with some traces of opaque and talc minerals (less than 10%). Talc mineral occurs as coarse grains outlined in a matrix of calcite. Few pores and micro-discontinuities were observed in this rock. ZK02-H1 specimens consisted of calcite as a major mineral constituent, with some accessory minerals such as talc and quartz (less than 5%). Talc and quartz are fine- to medium-grained textures. Very few microcracks were observed in this rock. Finally, limestone samples of ZK02-H2 are fine- to medium-grained texture and are composed of calcite as their main mineral constituent, which was associated with some traces of minerals including talc and magnesite. Small amounts of fine fossils were presented in these samples.

Table 1. Results of X-ray diffraction (XRD) and petrographic analysis for studied samples.

Rock Type	Code	Mineralogical Composition	Photomicrograph
Limestone.1	CK-H1	 <p>Major: Ce: Calcite</p>	
Limestone.2	ZK01-H1	 <p>Major: Ce: Calcite</p>	
Limestone.3	ZK01-H2	 <p>Major: Ce: Calcite Traces: T: Talc</p>	
Limestone.4	ZK02-H1	 <p>Major: Ce: Calcite Traces: T: Talc Q: Quartz</p>	
Limestone.5	ZK02-H2	 <p>Major: Ce: Calcite Traces: T: Talc Hy: Magnesite</p>	

2.3. Frost Attack Process

Frost action is the atmospheric influence due to seasonal environmental conditions. For this reason, rock materials used for construction partially or completely deteriorate. When the temperature falls below the freezing point, water in the discontinuities and fractures of the rock increases stresses on the surface of these fractures and result in an increase in volume. Repeating this process causes degradation of materials [32,33]. An automatic freezing–thawing machine, Wuhan, China was used in

this study. Frost attack cycles were carried out according to the test methods procedures outlined by DL/T 5368–2007, the Professional Standard Compilation Group of the People’s Republic of China [34]. The rock samples were exposed to cycles of freezing at $-20\text{ }^{\circ}\text{C}$ and thawing at $20\text{ }^{\circ}\text{C}$. Samples were saturated in distilled water beforehand for 48 h and then spent 4 h in a freezing chamber, followed by 4 h in distilled water at $20\text{ }^{\circ}\text{C}$. This process is named one frost cycle and it was repeated to a total of 50 times. At the end of 10, 20, 30, 40, and 50 cycles, the unconfined compressive strength and some nondestructive engineering parameters (including porosity, compressional wave velocity, and spatial attenuation) were obtained.

2.4. Unconfined Compression Test

The unconfined compression strength test was performed on core specimens of 50 mm and a length of 100 mm following the requirements of ISRM outlined methods and some references [35–40]. In this study, we used a self-designed TAW-2000 microcomputer electro-hydraulic servo-controlled testing system. The maximum capacity of the system was 2000 kN with loading rate of 0.1kN/s and an accuracy of $\pm 1\%$. The opposite side surfaces of the rock specimens were ground and flattened so that they were parallel to each other and perpendicular to the specimen axis. Therefore, the load could be applied uniformly. The test was carried out after every 10 cycles of frost. Thirty samples were used in this test, and their mean value and standard deviation were determined.

2.5. Porosity and Water Absorption

The porosity and water absorption were measured according to the procedures suggested by ISRM [40] after the end of every 10 frost cycles. The presence of water strongly influences rock materials properties [41]. For this purpose, the porosity and absorption of water was determined using the saturation technique.

2.6. Ultrasonic System

Ultrasonic technique was carried out according to the test methods procedures outlined by Martínez-Martínez et al. [15]. In this study, we used a non-metal ultrasonic detector system with two transducers (one was transmitter for launching the ultrasonic wave pulse, and the other was the receiver for receiving the ultrasonic wave). The transducers frequency was centered in 1000 KHz. Ultrasonic tests were carried out on cylindrical samples with a diameter of 50 mm. The faces of specimens were smoothed and flattened, and then end surfaces of the cylindrical samples were covered with grease to achieve a good coupling between the transducer face and the specimen surface in order to maximize accuracy of the travel time measurement. The compressional wave velocity (V_p) and spatial attenuation (as) were determined from each recorded waveform. This test was performed on 30 samples (six samples for each type of rock). Compressional wave velocity is the most widely used ultrasonic property to evaluate engineering characteristics of the rock samples and it was calculated by using the transit time (μs) from the generator to a receiver at the opposite end and path length of specimen (cm). However, the spatial attenuation (as) is more critical and sensitive ultrasound properties to detect any degradation processes in materials and it was calculated using (1):

$$as\text{ (dB/cm)} = 20.\log (Ae/Amax)/L \quad (1)$$

where Ae is the maximum amplitude emitted by the transmitter sensor, $Amax$ is the maximum amplitude (in absolute values) recorded by the receptor sensor, and L is the length of the rock sample. This test was performed after the end of every 10 frost attack cycles, and the samples were dried between cycles. The mean values and standard deviation of ultrasonic measurements were obtained.

3. Results and Discussions

The mean values of the initial physical and mechanical properties of studied fresh limestone specimens (unweathered) are summarized in Table 2.

Table 2. Average values of dry bulk density (ρ_b), water absorption (Wa), effective porosity (Pe), compressional wave velocity (Vp), spatial attenuation (as), and unconfined compressive strength (σ_c) of fresh samples.

Rock Type	Code	ρ_b (Gr/cm ³)	Wa (%)	Pe (%)	Vp (km/s)	as (dB/cm)	σ_c (MPa)
Limestone 1	CK-H1	2.61	0.05	0.13	4.81	3.0	92.4
Limestone 2	ZK01-H1	2.61	0.13	0.32	4.76	3.23	83.70
Limestone 3	ZK01-H2	2.59	0.31	0.78	4.15	3.99	53.80
Limestone 4	ZK02-H1	2.60	0.26	0.65	4.39	3.56	69.70
Limestone 5	ZK02-H2	2.60	0.15	0.39	4.51	3.38	72.0

The unconfined compressive strength, porosity, compressional wave velocity, and spatial attenuation were obtained after the end of each 10 cycles. Thirty samples for each type of rock (Six samples for each 10 cycles), and their mean values and standard deviation are given in Tables 3–6, respectively. As can be seen, the greater the number of cycles, the greater the porosity and spatial attenuation and the lower the unconfined compressive strength and compressional wave velocity of all studied limestone samples. The relation between unconfined compressive strength (σ_c), compression wave velocity (Vp), and the number of cycles for studied samples is presented in Figures 1 and 2.

Table 3. Mean values and standard deviation (SD) of unconfined compressive strength for samples after frost cycles.

Cycles	Unconfined Compressive Strength σ_c (Mpa)									
	10		20		30		40		50	
	Mean	SD	Mean	SD	Mean	SD	Mean	SD	Mean	SD
CK-H1	90.8	10.2	88.6	11.1	88.0	8.6	85.8	12.3	84.0	13.1
ZK01-H1	81.9	8.9	80.8	10.8	80.5	11.7	75.7	13.8	73.6	13.4
ZK01-H2	48.1	11.9	45.1	12.6	43.6	13.8	40.1	10.2	32.8	14.6
ZK02-H1	67.0	14.6	66.6	13.2	65.3	14.9	61.8	13.6	56.9	15.6
ZK02-H2	67.5	12.3	65.0	13.9	60.8	10.6	60.0	14.1	58.7	11.5

Table 4. Mean values and standard deviation (SD) of effective porosity for samples after frost cycles.

Cycles	Effective Porosity Pe (%)									
	10		20		30		40		50	
	Mean	SD	Mean	SD	Mean	SD	Mean	SD	Mean	SD
CK-H1	0.15	0.02	0.17	0.01	0.17	0.03	0.20	0.01	0.22	0.04
ZK01-H1	0.39	0.03	0.47	0.04	0.55	0.06	0.60	0.03	0.67	0.06
ZK01-H2	1.05	0.05	1.24	0.07	1.39	0.04	1.51	0.07	1.70	0.08
ZK02-H1	0.78	0.02	0.88	0.03	1.04	0.05	1.10	0.04	1.26	0.06
ZK02-H2	0.46	0.01	0.53	0.03	0.60	0.05	0.65	0.03	0.73	0.05

Table 5. Mean values and standard deviation (SD) of compressional wave velocity for samples after frost cycles.

Compressional Wave Velocity V_p (km/s)										
Cycles	10		20		30		40		50	
	Mean	SD								
CK-H1	4.80	0.11	4.79	0.13	4.77	0.12	4.73	0.15	4.76	0.18
ZK01-H1	4.75	0.10	4.75	0.12	4.74	0.14	4.73	0.11	4.72	0.15
ZK01-H2	4.11	0.13	4.08	0.15	4.06	0.16	4.03	0.14	3.9	0.15
ZK02-H1	4.38	0.09	4.38	0.10	4.37	0.12	4.36	0.11	4.34	0.14
ZK02-H2	4.49	0.14	4.48	0.12	4.45	0.15	4.44	0.17	4.41	0.19

Table 6. Mean values and standard deviation (SD) of spatial attenuation for samples after frost cycles.

Spatial Attenuation α_s (dB/cm)										
Cycles	10		20		30		40		50	
	Mean	SD	Mean	SD	Mean	SD	Mean	SD	Mean	SD
CK-H1	3.02	0.01	3.04	0.02	3.05	0.04	3.07	0.01	3.08	0.05
ZK01-H1	3.26	0.03	3.28	0.05	3.31	0.06	3.33	0.05	3.35	0.06
ZK01-H2	4.04	0.01	4.08	0.03	4.13	0.02	4.17	0.04	4.22	0.07
ZK02-H1	3.59	0.02	3.61	0.04	3.64	0.03	3.65	0.04	3.68	0.05
ZK02-H2	3.40	0.03	3.43	0.01	3.47	0.04	3.52	0.05	3.544	0.07

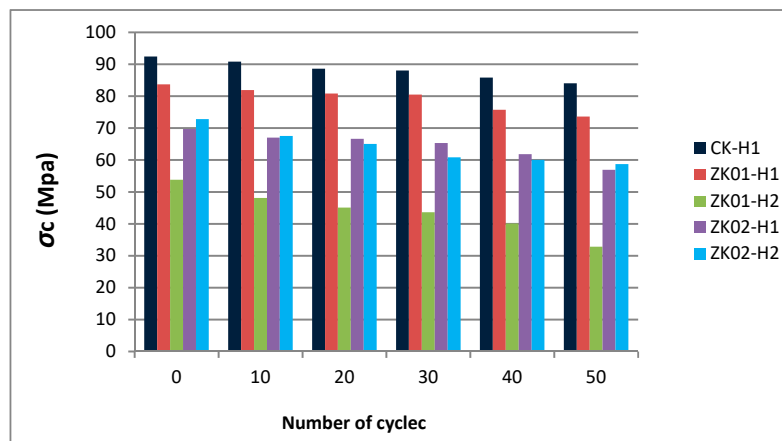


Figure 1. Relationship between σ_c and N .

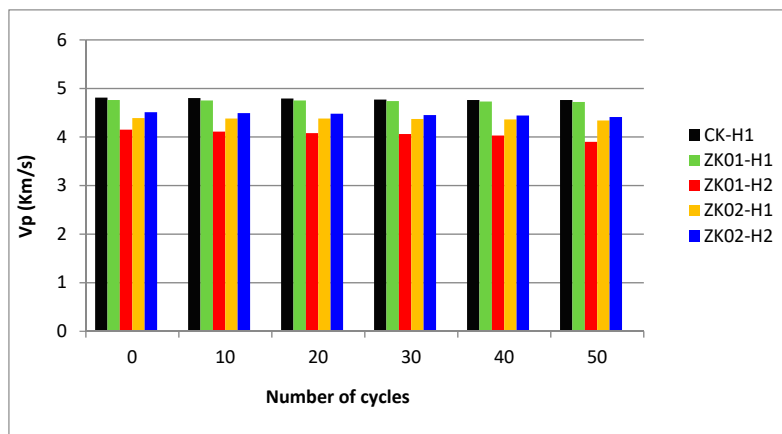


Figure 2. Relationship between V_p and N .

To indicate the variation in critical parameters, the change ratios of unconfined compressive strength, porosity, compressional wave velocity, and spatial attenuation were obtained. The rate of increase and decrease determines the degree of rock material breakage and it changed between 0 and 1. A rating value of 1 was assigned to rocks that were fully damaged after the end of 50 frost cycles. The increase in ratios of an effective porosity and spatial attenuation after the end of every 10 frost cycles was determined using Formula (2) outlined by Khanlari et al. [8]:

$$RI = (r_n/r_o) - 1 \quad (2)$$

where RI is the increase ratio of a property (effective porosity, and spatial attenuation), r_n is the property after the end of each 10 frost cycles, and r_o is the property value of fresh specimens. The relationship between the increase ratio values of effective porosity (RI_{pe}) and the number of frost cycles of studied samples (N) are indicated in Figure 3. As can be observed in this Figure, after 50 cycles of frost action, ZK01-H2 and ZK01-H1 limestone samples indicate the highest increase ratio in porosity (RI_{pe}), with 1.1795 and 1.0983, respectively, in comparison with the other specimens. Limestone samples of ZK02-H1 and ZK02-H2 show slightly higher increased ratio in porosity with 0.9385 and 0.8718, respectively, whereas CK-H1 limestone samples exhibit the lowest increase ratio with 0.6923 in comparison with the other specimens. These variations are considered to be related to the mineralogical composition of these specimens, especially calcium carbonate (calcite) mineral, which exhibits a higher expansion–contraction property in the frost weathering action, and these changes lead to rock breakage or deterioration [42]. According to the degree of variation due to the frost attack process, new cracks or fractures have been observed in limestone samples (namely ZK01-H2). As shown in Figure 1, there were slightly higher changes in the ZK01-H2 specimens after the 10th to 40th cycle, while in other samples, RI_{pe} increased with the increased number of frost cycles.

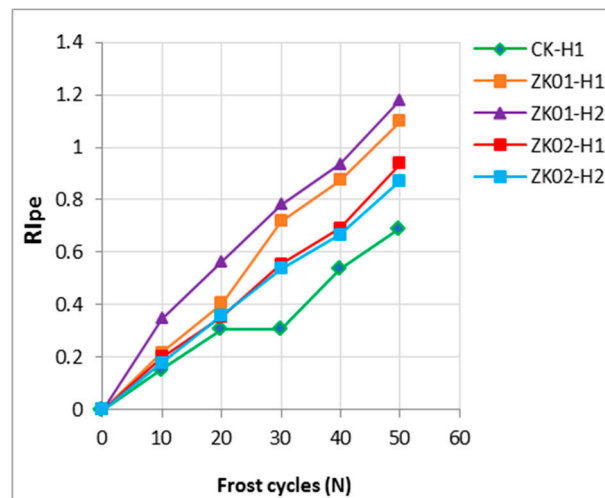


Figure 3. Relationship between RI_{pe} and N .

On the other hand, the relationship between RI_{as} and number of frost cycles of specimens (N) are illustrated in Figure 4. As can be seen, after 50 cycles of frost, ZK01-H2 samples have the highest increase ratio in spatial attenuation (RI_{as}), with 0.0630 compared to other samples, while ZK02-H2, ZK01-H1, and ZK02-H1 samples have increased ratios of spatial attenuation with 0.0490, 0.0370, and 0.0340, respectively. Finally, CK-H1 samples have the lowest increase ratio, with 0.0270 compared to other samples. Artificial weathering tests led to internal disintegration of rock materials, which scatters the ultrasound waves and results in increase of spatial attenuation [14]. Therefore, the variation degree of these parameters depends on internal deterioration degree of the rock material [43], which determines the durability of materials. Depending on these results, it can be said that the ZK01-H2 samples have the lowest durability due to having the highest values of RI_{as} , while CK-H1 samples

have the highest durability because RI_{as} has the lowest values for these samples due to frost process. As shown in Figure 4, RI_{as} increases with an increased number of frost weathering cycles of studied limestone samples.

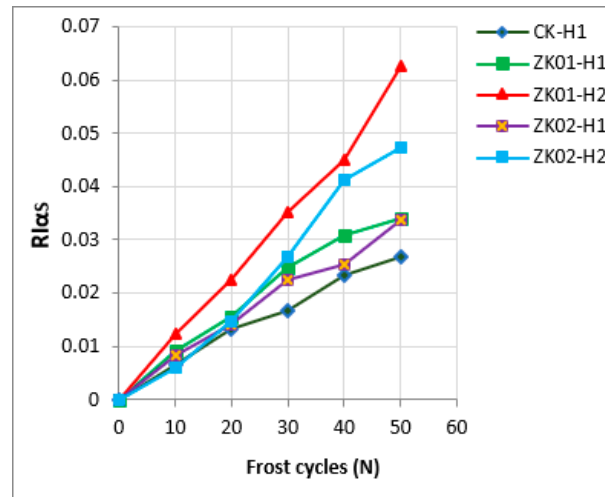


Figure 4. Relationship between RI_{as} and N .

The high absorption of water, breakage, or disintegration and the weakening and expansion of natural rocks led to the development and formation of microfractures and cracks due to frost action, and hence, the reduction in the strength of the stones is higher. The decrease in ratios of the unconfined compressive strength and the compressional wave velocity after the end of each 10 cycles of frost were determined using Equation (3),

$$RD = 1 - (r_n/r_o) \quad (3)$$

where RD is the decrease ratio of the property (unconfined compressive strength, and compressional wave velocity), r_n is the property after the end of each 10 frost cycles, and r_o is the initial property of fresh sample. The relationship between the decrease ratios in unconfined compressive strength (RD_{σ_c}), compressional wave velocity (RD_{vp}) values, and the number of frost cycles of specimens (N) are given in Figures 5 and 6, respectively. It is observed that the progression of the frost cycles caused reduction in unconfined compressive strength and compressional wave velocity. According to Mokhtari and Behnia [44], there are some critical parameters affected on the rock materials strength and elasticity including rock type, mineralogical composition, porosity and water absorption capacity. As can be seen in Figure 5, after 50 cycles of frost action, ZK01-H2 specimens have the highest decrease in unconfined compressive strength value (RD_{σ_c}) with 0.3903 and hence the highest deterioration because of their higher porosity and water absorption in addition the noticeable presence of talc mineral. Therefore, ZK01-H2 is the most sensitive to frost process in comparison with the other samples. Ruedrich et al. [45] indicated that the water and moisture content of natural rock materials are significant factors during frost action. Wet freezing–thawing process proceedings are considered limited because natural rock materials have to be moistened before frost action. The presence of water in the rocks is an important parameter for the damage action [46].

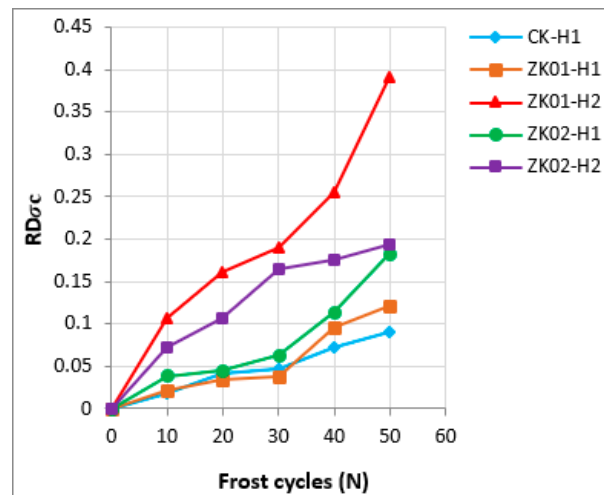


Figure 5. Relationship between $RD_{\sigma c}$ and N .

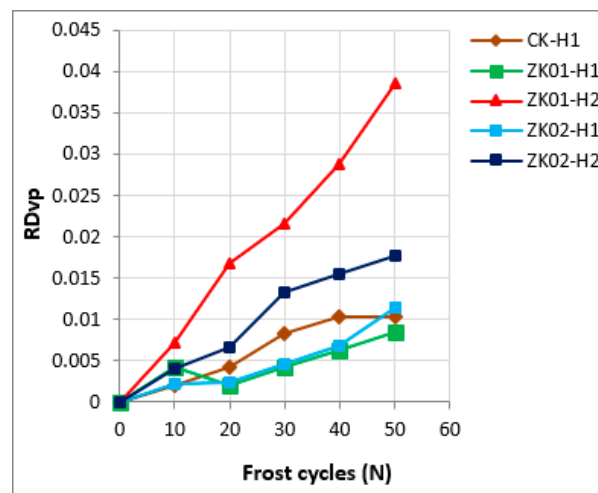


Figure 6. Relationship between RD_{vp} and N .

On the other hand, limestone samples of CK-H1 exhibit the highest resistance to deterioration because these samples have the lowest value of $RD_{\sigma c}$ with 0.0909 due to having the lowest moisture content and porosity under frost weathering action in comparison with the other samples. Erguvan [47] showed that the percentage reduction in uniaxial compressive strength must be less than 20% for rocks used as building materials. If the reduction value of these materials is more than 20%, they should not be used in cold areas. Depending on these results, most studied samples can be used in cold areas as building and construction materials except limestone samples namely ZK01-H2 should not be used in cold areas due to having high percentage reduction in unconfined compressive strength.

Figure 6 presents the relationship between the decrease ratio values of compressional wave velocity (RD_{vp}) and the number of frost cycles of specimens (N). After 50 cycles of frost, limestone samples of ZK01-H2 have the highest decrease in compressional wave velocity value (RD_{vp}) with 0.0386, which resulted in the highest internal deterioration in comparison with the other samples while, samples of CK-H1 have the highest resistance to damage due to having the lowest RD_{vp} value with 0.0104 compared to the other samples. The reduction in index properties of rock materials after frost cycles are found to be closely related initial index parameters including porosity, absorption of water, and mineralogical composition. Accelerated weathering processes lead to rock material breakage or degradation and result in variation in the index characteristics of the rocks [42]. According to the present results, it is observed that high porosity, water absorption, and mineralogical composition are

critical characteristics for determining the strength loss of studied limestone samples against frost attack processes.

Relationships Evolution between $RD\sigma c$ and Limestone Properties Variations

The correlation diagrams were used to investigate the relationships between decrease rate of unconfined compressive strength ($RD\sigma c$) and other nondestructive physical characteristics variations of studied samples, including the increase ratio in porosity ($RIpe$) and spatial attenuation ($RI\alpha s$) and the decrease ratio in compressional wave velocity ($RDvp$) realized due to frost attack cycles. Moreover, we attempt to find the higher correlation between these parameters. The dataset was analyzed using linear regression analysis and the coefficient of determination (R^2) was determined for each regression. Correlation coefficient was determined to assess the strength and direction of the correlations the correlation between $RD\sigma c$ and the other disintegration parameters.

Figures 7–11 present the relationships between $RD\sigma c$ and $RIpe$ & $RI\alpha s$ at 10, 20, 30, 40, and 50 cycles, respectively, and the relationships between $RD\sigma c$ and $RDvp$ are illustrated in Figures 12–16.

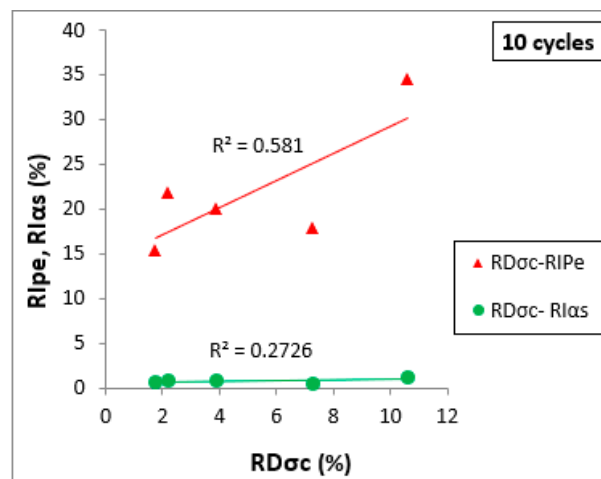


Figure 7. Relationship between $RD\sigma c$ and $RIpe$ & $RI\alpha s$ at 10 cycles.

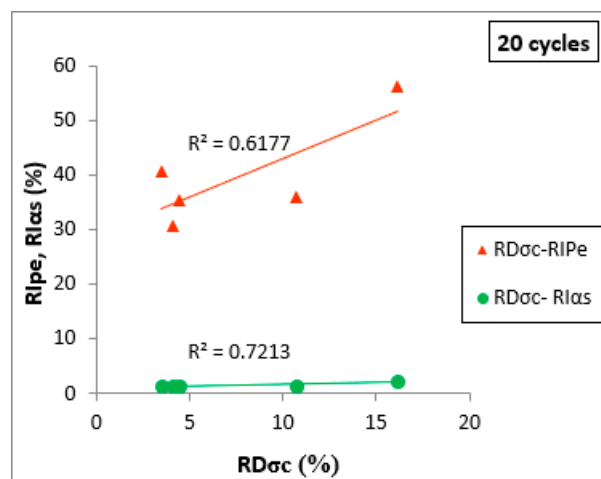


Figure 8. Relationship between $RD\sigma c$ and $RIpe$ & $RI\alpha s$ at 20 cycles.

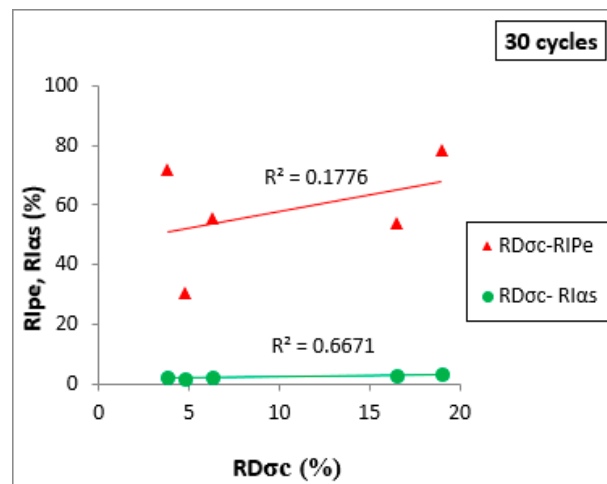


Figure 9. Relationship between $RD\sigma c$ and $Ripe$ & $RIas$ at 30 cycles.

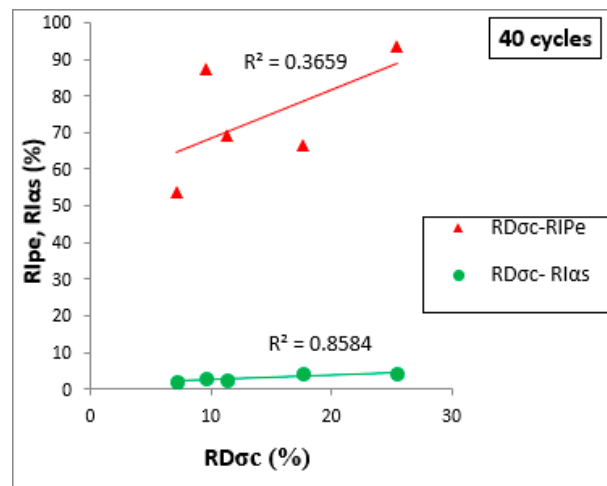


Figure 10. Relationship between $RD\sigma c$ and $Ripe$ & $RIas$ at 40 cycles.

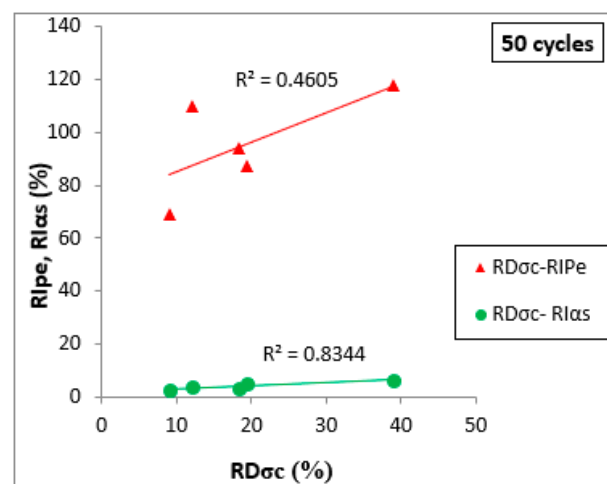


Figure 11. Relationship between $RD\sigma c$ and $Ripe$ & $RIas$ at 50 cycles.

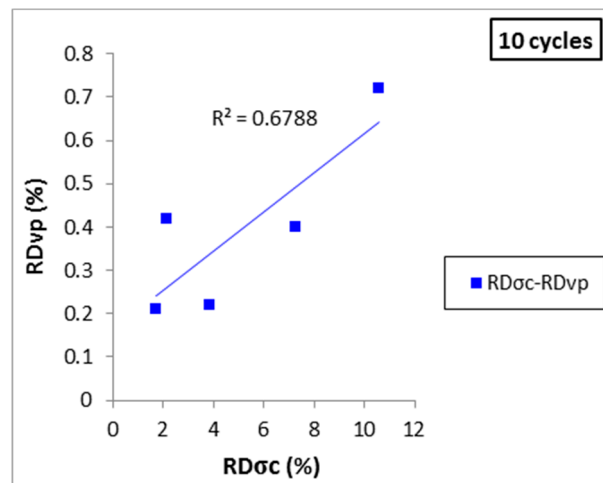


Figure 12. Relationship between $RD\sigma_c$ and $RDvp$ at 10 cycles.

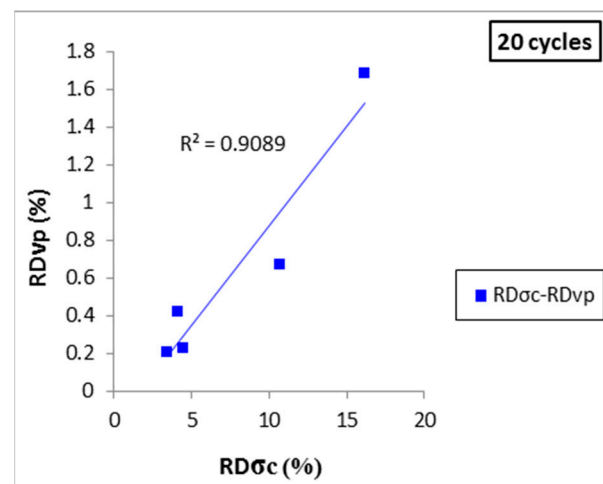


Figure 13. Relationship between $RD\sigma_c$ and $RDvp$ at 20 cycles.

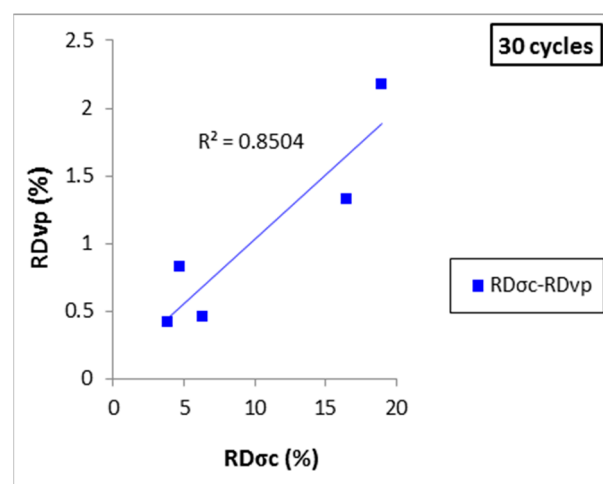


Figure 14. Relationship between $RD\sigma_c$ and $RDvp$ at 30 cycles.

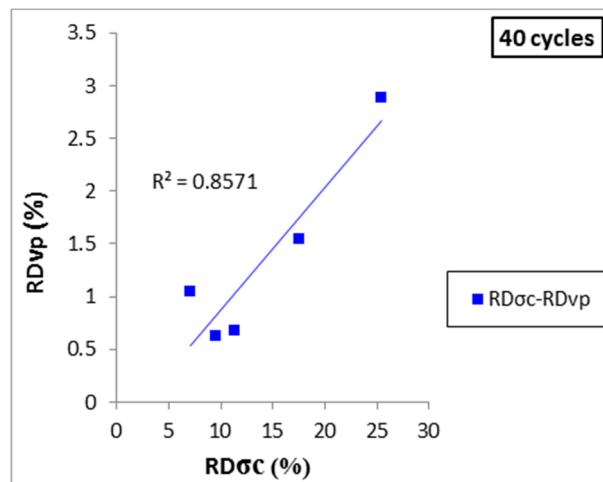


Figure 15. Relationship between $RD\sigma_c$ and $RDvp$ at 40 cycles.

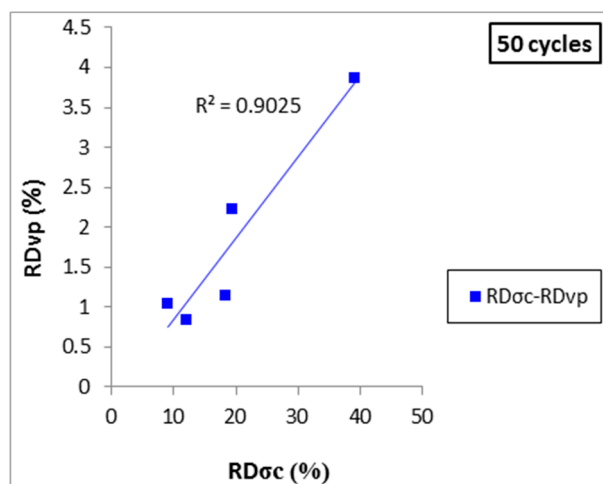


Figure 16. Relationship between $RD\sigma_c$ and $RDvp$ at 50 cycles.

As can be observed in Figures 7–11, there are no significant correlations between $RD\sigma_c$ and $RIpe$. As these Figures show, the low values of their coefficients of determination (R^2) and hence the correlation between them is poor. As shown in these diagrams, depending on the number of cycles, a moderately correlation was observed between $RD\sigma_c$ and $RIpe$ after the end of the 10th and 20th cycles of frost. The moderate values of their coefficients of determination with R^2 of 0.58 and 0.61, respectively. In addition, their scatter plots show that some points are close to the regression lines and the others are far and thus the correlation between them are moderate. The progression of frost cycles caused a decrease in relationship between $RD\sigma_c$ and $RIpe$. The greater the number of cycles, the lower the correlation coefficients. Figures 10 and 11 indicate that there is a strong correlation between $RD\sigma_c$ and $RIas$ with large values of R^2 of 0.8584 and 0.8344, respectively, after the end of 40th and 50th frost cycles, and their scatter plots indicate that the stronger the relationship, the closer the data points fall to the regression lines also, which corresponds to the best fitting linear relationship for obtaining the decrease of unconfined compressive strength. It is observed that the progression of frost cycles led to increase in relationship between $RD\sigma_c$ and $RIas$. These higher relationships indicate that the increase ratio of spatial attenuation ($RIas$) is a more sensitive ultrasound parameter for detecting any degradation processes and formation of new microcracks in materials during frost processes (depending on the number of frost cycles). Therefore, the highest relationship between $RD\sigma_c$ and $RIas$ can be used for pre-estimation of unconfined compressive strength loss ($RD\sigma_c$) for studied limestone types.

As can be seen in Figures 12–16, the further the progression of frost cycles, the higher the relationship between $RD\sigma_c$ and RDv_p . Figures 13 and 16 indicate that there is a strong correlation between $RD\sigma_c$ and RDv_p with R^2 of 0.9089 and 0.9025, respectively, at the end of 20th and 50th frost cycles. Consequently, these relations are a strong indicator for pre-determining the unconfined compression strength loss of studied samples.

These correlations also represent a positive and linear relationship. According to the number of cycles, it can be observed that the increase rate of spatial attenuation (RIa_s) and the decrease rate of compressional wave velocity (RDv_p) are very sensitive for analyzing the fabric deterioration of limestone samples against frost weathering processes.

Therefore, the ultrasonic detection system is a powerful technique for investigating the durability of studied samples during frost attack processes. Overall, it is concluded that the RIa_s factor related to spatial attenuation obtained at the end of 40th frost attack cycles can be used to estimate the unconfined compressive strength ($RD\sigma_c$) reduction. Moreover, RDv_p parameter related to compressional wave velocity decrease determined at the end of 20th and 50th cycles of frost can be used for pre-estimation of unconfined compressive strength decrease of selected studied samples without tests. These relations may be useful at the preliminary stage of design but should be used with caution and only for the selected samples. The results also support the use of nondestructive tests and provide valuable data when choosing limestone samples.

4. Conclusions

The employment of nondestructive methods to determine the mechanical strength and durability of carbonate building and construction materials under frost conditions is gaining great significance. For this purpose, the present study aimed to determine the relationships between unconfined compressive strength decrease and some nondestructive physical parameters variations including the increase ratios of porosity and spatial attenuation and the decrease ratios of compressional wave velocity of some limestone types used as building and construction materials and subjected to 50 frost attack cycles. This provided useful information for the assessment of their long-term durability in order to ensure the long-term viability or sustainability of these materials used for constructions under frost action.

The main conclusions drawn from the present study can be summarized as follow:

(1) Most of studied limestone samples can be used as building and construction materials for different outdoor applications in severe cold areas, except ZK01-H2.

(2) The high porosity, water absorption capacity, and presence of some accessory minerals such as talc are critical parameters for determining the strength losses of samples from nondestructive physical parameter changes against frost attack processes.

(3) There is a high linear relationship between $RD\sigma_c$ and RIa_s at 40th frost cycles with R^2 of 0.8584. Moreover, there is also a strong linear correlation between $RD\sigma_c$ and RDv_p at the end of 20th and 50th frost cycles with R^2 of 0.9089 and 0.9025. Consequently, the ultrasound measurements including compressional wave velocity decrease and spatial attenuation increase factors can be successfully used to pre-determine the unconfined compression strength loss of only the studied limestone types against frost conditions without testing. It also may be useful at the preliminary stage of design but should be used with caution and only for limestone types in many engineering applications in cold regions.

This study also creates a paradigm for future studies for pre-estimation of unconfined compressive strength loss of studied limestone used as building materials subject to frost weathering. However, to evaluate the relations between materials characteristics clearly, future studies need to use different conditions and construction materials in order to obtain more important results.

Author Contributions: Methodology, M.M.A.A. and G.R.; Formal analysis, M.M.A.A.; Writing—original draft preparation, D.L.; Writing—review and editing, M.M.A.A.; Funding acquisition, G.R. All authors have read and agreed to the published version of the manuscript.

Funding: This research was supported by the National Key R&D Plan under Grant No. 2018YFC0808405 and No. 2018YFC0604401 and the Natural Science Foundation of China under Grant No. 51774220.

Acknowledgments: The authors are very grateful for the support of the fund.

Conflicts of Interest: The authors declare no conflict of interest.

References

1. Yu, J.; Chen, X.; Li, H.; Zhou, J.; Cai, Y. Effect of freeze–thaw cycles on mechanical properties and permeability of red sandstone under triaxial compression. *J. Mt. Sci.* **2015**, *12*, 218–231. [[CrossRef](#)]
2. Grossi, C.M.; Brimblecombe, P.; Harris, I. Predicting long term freeze–thaw risks on Europe built heritage and archaeological sites in a changing climate. *Sci. Total Environ.* **2007**, *377*, 273–281.
3. Singer, D.A.; Bliss, J.D. Use of a Probabilistic Neural Network to Reduce Costs of Selecting Construction Rock. *Nat. Resour. Res.* **2003**, *12*, 135–140. [[CrossRef](#)]
4. Zhou, Z.; Cai, X.; Chen, L.; Cao, W.; Zhao, Y.; Xiong, C. Influence of cyclic wetting and drying on physical and dynamic compressive properties of sandstone. *Eng. Geol.* **2017**, *220*, 1–12. [[CrossRef](#)]
5. Zhou, Z.; Cai, X.; Ma, D.; Chen, L.; Wang, S.; Tan, L. Dynamic tensile properties of sandstone subjected to wetting and drying cycles. *Constr. Build. Mater.* **2018**, *182*, 215–232. [[CrossRef](#)]
6. Jamshidi, A.; Nikudel, M.R.; Khamsehchiyan, M. Predicting the long-term durability of building stones against freeze–thaw using a decay function model. *Cold Reg. Sci. Technol.* **2013**, *92*, 29–36. [[CrossRef](#)]
7. Zhang, S.J.; Lai, Y.M.; Zhang, X.F.; Pu, Y.B.; Yu, W.B. Study on the damage propagation of surrounding rock from a cold-region tunnel under freeze–thaw cycle condition. *Tunn. Space. Technol.* **2004**, *19*, 295–302. [[CrossRef](#)]
8. Khanlari, G.; Sahamieh, R.Z.; Abdilor, Y. The effect of freeze–Thaw cycles on physical and mechanical properties of Upper Red Formation sandstones, central part of Iran. *Arab J. Geosci.* **2015**, *8*, 5991–6001. [[CrossRef](#)]
9. Jamshidi, A.; Nikudel, M.R.; Khamsehchiyan, M. Evaluation of the durability of Gerdoee travertine after freeze–thaw cycles in fresh water and sodium sulfate solution by decay function models. *Eng. Geol.* **2016**, *202*, 36–43. [[CrossRef](#)]
10. Takarli, M.; Prince, W.; Siddique, R. Damage in granite under heating/cooling cycles and water freeze–thaw condition. *Int. J. Rock Mech. Min. Sci.* **2008**, *45*, 1164–1175. [[CrossRef](#)]
11. Tuğrul, A. The effect of weathering on the pore geometry and compressive strength of selected rock types from Turkey. *Eng. Geol.* **2004**, *75*, 215–227. [[CrossRef](#)]
12. Chen, T.C.; Yeung, M.R.; Mori, N. Effect of water saturation on deterioration of welded tuff due to freeze–thaw action. *Cold Reg. Sci. Technol.* **2004**, *38*, 127–136. [[CrossRef](#)]
13. Bayram, F. Predicting mechanical strength loss of natural stones after freeze–thaw in cold regions. *Cold Reg. Sci. Technol.* **2012**, *83–84*, 98–102. [[CrossRef](#)]
14. Fort, R.; Alvarez de Buergo, M.; Perez-Monserrat, E.M. Nondestructive testing for the assessment of granite decay in heritage structures compared to quarry stone. *Int. J. Rock Mech. Min. Sci.* **2013**, *61*, 296–305. [[CrossRef](#)]
15. Martínez-Martínez, J.; Benavente, D.; García-del-Cura, M.A. Spatial attenuation: The most sensitive ultrasonic parameter for detecting petrographic features and decay processes in carbonate rocks. *Eng. Geol.* **2011**, *119*, 84–95. [[CrossRef](#)]
16. Martínez-Martínez, J.; Benavente, D.; Gomez-Heras, M.; Marco-Castaño, L.; García-del-Cura, M.A. Non-linear decay of building stones during freeze–thaw weathering processes. *Constr. Build. Mater.* **2013**, *38*, 443–454. [[CrossRef](#)]
17. Hashemi, M.; Goudarzi, M.B.; Bashiri, A.; Jamshidi, A. Experimental investigation on the performance of Schmidt hammer test in durability assessment of carbonate building stones against freeze–thaw weathering. *Environ. Earth Sci.* **2018**, *77*, 684. [[CrossRef](#)]
18. Yavuz, H.; Altindag, R.; Sarac, S.; Ugur, I.; Sengun, N. Estimating the index properties of deteriorated carbonate rocks due to freeze–thaw and thermal shock weathering. *Int. J. Rock Mech. Min. Sci.* **2006**, *43*, 767–775. [[CrossRef](#)]
19. Saad, A.; Guedon, S.; Martineau, F. Microstructural Weathering of Sedimentary Rocks by Freeze–Thaw Cycles: Experimental Study of State and Transfer Parameters. *Comptes. Rendus Geosci.* **2010**, *342*, 197–203. [[CrossRef](#)]

20. Karaca, Z.; Oztank, N.; Gokce, M.V.; Elci, H. Effects of Surface-Finishing Forms and Cement-Filling on Porous Dimension Limestone Deterioration in Cold Regions. *Cold Reg. Sci. Technol.* **2011**, *68*, 124–129. [[CrossRef](#)]
21. Tan, X.; Chen, W.; Tian, H.; Cao, J. Laboratory Investigations on the Mechanical Properties Degradation of Granite under Freeze–Thaw Cycles. *Cold Reg. Sci. Technol.* **2011**, *68*, 130–138. [[CrossRef](#)]
22. Mutluturk, M.; Altindag, R.; Turk, G. A decay function model for the integrity loss of rock when subjected to recurrent cycles of freezing–thawing and heating–cooling. *Int. J. Rock Mech. Min. Sci.* **2004**, *41*, 237–244. [[CrossRef](#)]
23. Sousa, L.M.O.; Suarez del Rio, L.M.; Calleja, L.; Ruiz de Argondona, V.G.; Rey, A.R. Influence of microfractures and porosity on the physico-mechanical properties and weathering of ornamental granites. *Eng. Geol.* **2005**, *77*, 153–168. [[CrossRef](#)]
24. Baud, P.; Wong, T.F.; Zhu, W. Effects of porosity and crack density on the compressive strength of rocks. *Int. J. Rock Mech. Min. Sci.* **2014**, *67*, 202–2011. [[CrossRef](#)]
25. Momeni, A.; Abdilor, Y.; Khanlari, G.; Heidari, M.; Sepahi, A. The effect of freeze–Thaw cycles on physical and mechanical properties of granitoid hard rocks. *Bull. Eng. Geol. Environ.* **2016**, *75*, 1649–1656. [[CrossRef](#)]
26. Ghobadi, M.H.; Babazadeh, R. Experimental studies on the effects of cyclic freezing–Thawing, salt crystallization, and thermal shock on the physical and mechanical characteristics of selected sandstones. *Rock Mech. Rock. Eng.* **2015**, *48*, 1001–1016. [[CrossRef](#)]
27. Iñigo, A.C.; García-Talegón, J.; Vicente-Tavera, S.; Martín-González, S.; Casado-Marina, S.; Vargas-Muñoz, M.; Pérez-Rodríguez, J.L. Colour and ultrasound propagation speed changes by different ageing of freezing/thawing and cooling/heating in granitic materials. *Cold Reg. Sci. Technol.* **2013**, *85*, 71–78. [[CrossRef](#)]
28. Liu, Q.; Huang, S.; Kang, Y.; Liu, X. A prediction model for uniaxial compressive strength of deteriorated rocks due to freeze–thaw. *Cold Reg. Sci. Technol.* **2015**, *120*, 96–107. [[CrossRef](#)]
29. Diamantis, K.; Gartzos, E.; Migiros, G. Study on uniaxial compressive strength, point load strength index, dynamic and physical properties of serpentinites from Central Greece: Test results and empirical relations. *Eng. Geol.* **2009**, *108*, 199–207. [[CrossRef](#)]
30. Xu, G.; Liu, Q. Analysis of mechanism of rock failure due to freeze–thaw cycling and mechanical testing study on frozen–thawed rocks. *Chin. J. Rock Mech. Eng.* **2005**, *17*, 3076–3082.
31. Hale, P.A.; Shakoor, A. A laboratory investigation of the effects of cyclic heating and cooling, wetting and drying and freezing and thawing on the compressive strength of selected sandstones. *Environ. Eng. Geosci.* **2003**, *9*, 117–130. [[CrossRef](#)]
32. Yavuz, A.B.; Akal, C.; Turk, N.; Colak, M.; Tanyu, B.F. Investigation of discrepancy between tuff used as building stones in historical and modern buildings in western Turkey. *Constr. Build. Mater.* **2015**, *93*, 439–448. [[CrossRef](#)]
33. Fener, M.; Ince, I. Effects of the freeze–thaw (F–T) cycle on the andesitic rocks (Sille-Konya/Turkey) used in construction building. *J. Afr. Earth Sci.* **2015**, *109*, 96–106. [[CrossRef](#)]
34. *National Development and Reform Commission of the People’s Republic of China, Code for Rock Tests of Hydroelectric and Water Conservancy Engineering (DL/T 5368-2007)*; National Development and Reform Commission of the People’s Republic of China: Beijing, China, 2007; pp. 11–12.
35. Zhou, Y.X.; Xia, K.; Li, X.B.; Li, H.B.; Ma, G.W.; Zhao, J.; Zhou, Z.L.; Dai, F. Suggested methods for determining the dynamic strength parameters and mode-I fracture toughness of rock materials. *Int. J. Rock Mech. Min. Sci.* **2014**, *35*–44. [[CrossRef](#)]
36. Zhou, Z.; Cai, X.; Li, X.; Cao, W.; Du, X. Dynamic response and energy evolution of sandstone under coupled static–dynamic compression: Insights from experimental study into deep rock engineering applications. *Rock Mech. Rock. Eng.* **2019**, 1–27. [[CrossRef](#)]
37. Kou, M.; Liu, X.; Tang, S.; Wang, Y. 3-D X-ray computed tomography on failure characteristics of rock-like materials under coupled hydro-mechanical loading. *Theor. Appl. Fracture Mech.* **2019**, *104*, 102396. [[CrossRef](#)]
38. ISRM; Ulusay, R.; Hudson, J. (Eds.) *The Complete ISRM Suggested Methods for Rock Characterization, Testing and Monitoring (1974–2006)*. *Int. Soc. Rock Mech.* **2007**.
39. Fairhurst, C.E.; Hudson, J.A. Draft ISRM suggested method for the complete stress strain curve for intact rock in uniaxial compression. *Int. J. Rock Mech. Min. Sci.* **1999**, *36*, 279–289.
40. ISRM. *Rock Characterization, Testing, and Monitoring. ISRM Suggested Methods*; Pergamon Press: Oxford, UK, 1981.

41. Cai, X.; Zhou, Z.; Liu, K.; Du, X.; Zang, H. Water-weakening effects on the mechanical behavior of different rock types: Phenomena and mechanisms. *Appl. Sci.* **2019**, *9*, 4450. [[CrossRef](#)]
42. Sarici, D.E.; and Ozdemir, E. Determining point load strength loss from porosity, Schmidt hardness, and weight some sedimentary rocks under freeze–thaw conditions. *Environ. Earth Sci.* **2018**, *77*, 62. [[CrossRef](#)]
43. Sun, H.; Sun, Q.; Deng, W.; Zhang, W.; Lü, C. Temperature effect on microstructure and P-wave propagation in Linyi sandstone. *Appl. Therm. Eng.* **2017**, *115*, 913–922. [[CrossRef](#)]
44. Mokhtari, M.; Behnia, M. Comparison of LLNF, ANN, and COA-ANN Techniques in Modeling the Uniaxial Compressive Strength and Static Young’s Modulus of Limestone of the Dalan Formation. *Nat. Resour. Res.* **2019**, *28*, 223–239. [[CrossRef](#)]
45. Ruedrich, J.; Kirchner, D.; Siegesmund, S. Physical weathering of building stones induced by freeze-thaw action: A laboratory long-term study. *Environ. Earth Sci.* **2011**, *63*, 1573–1586. [[CrossRef](#)]
46. De Kock, T.; Turmel, A.; Fronteau, G.; Cnudde, V. Rock fabric heterogeneity and its influence on the petrophysical properties of a building limestone: Lede stone (Belgium) as an example. *Eng. Geol.* **2017**, *216*, 31–41. [[CrossRef](#)]
47. Erguvanli, K. *Engineering Geology*; Sec Publication: Istanbul, Turkey, 1995; Volume 43.



© 2020 by the authors. Licensee MDPI, Basel, Switzerland. This article is an open access article distributed under the terms and conditions of the Creative Commons Attribution (CC BY) license (<http://creativecommons.org/licenses/by/4.0/>).